Hindawi
International Transactions on Electrical Energy Systems
Volume 2022, Article ID 4242996, 18 pages
https://doi.org/10.1155/2022/4242996

Research Article

Voltage Quality Enhancement of Low-Voltage Smart Distribution System Using Robust and Optimized DVR Controllers: Application of the Harris Hawks Algorithm

Mohamed Metwally Mahmoud,[1] **Yahia M. Esmail**,[2] **Basiony Shehata Atia**,[3] **Omar Makram Kamel**,[4] **Kareem M. AboRas**,[5] **Mohit Bajaj**,[6] **Syed Sabir Hussain Bukhari**,[7] **and Daniel Eutyche Mbadjoun Wapet**[8]

[1]*Electrical Engineering Department, Faculty of Energy Engineering, Aswan University, Aswan 81528, Egypt*
[2]*Ministry of Electricity and Renewable Energy, Cairo, Egypt*
[3]*Rapiscan Systems, 2805 Columbia St, Torrance, CA 90503, USA*
[4]*Electrical Engineering and Computers Department, El-Minya HIET, Minia, Egypt*
[5]*Department of Electrical Power and Machines, Faculty of Engineering, Alexandria University, Alexandria, Egypt*
[6]*Department of Electrical Engineering, Graphic Era (Deemed to Be University), Dehradun-248002, India*
[7]*School of Electrical and Electronics Engineering, Chung-Ang University, Dongjak-gu, Seoul 06974, Republic of Korea*
[8]*National Advanced School of Engineering, Université de Yaoundé I, Yaoundé, Cameroon*

Correspondence should be addressed to Mohit Bajaj; mohitbajaj@nitdelhi.ac.in and Daniel Eutyche Mbadjoun Wapet; eutychedan@gmail.com

Received 8 September 2022; Revised 10 October 2022; Accepted 18 October 2022; Published 17 November 2022

Academic Editor: Subrata Kumar Sarker

Copyright © 2022 Mohamed Metwally Mahmoud et al. This is an open access article distributed under the Creative Commons Attribution License, which permits unrestricted use, distribution, and reproduction in any medium, provided the original work is properly cited.

The voltage quality (VQ) index has become a significant measure of recent power system stability. The integration of photovoltaic (PV) systems plus smart home loads (SHLs) at low voltage levels (LVLs) has resulted in various issues such as harmonics rise and voltage instabilities as a result of faults and systems nonlinearity. In this work, a dynamic voltage resistor (DVR) is implemented to enhance VQ, and its dynamic performance hinges on its control system ability. To enhance the DVR's control system, for surpassing nonstandard voltage with a quick response and harmonics reduction at LVL under harsh operating events, an optimal controller design using the Harris Hawks algorithm (HHA) is proposed. To verify the value of the suggested solution, the hard operating events (voltage sag, voltage swell, fluctuating voltage, and imbalanced voltage) are examined and assessed. To show the effectiveness of the HHA technique, a comparison of the % total harmonic distortion (THD) reductions achieved by the suggested and conventional controllers of DVR is conducted for the scenarios under study. Moreover, the suggested controller stability is analyzed and assessed using Lyapunov's function. The benefits of the optimized controller system are inferred from the results, including their robustness, simplicity, efficient harmonic rejection, minimal tracking error, quick response, and sinusoidal reference track. The results of the simulation show that the DVR's optimized controller is efficient and effective in maintaining a voltage at the needed level with low THD, safeguarding the sensitive load as expected, and showing a noticeable improvement in voltage waveforms. The mathematical modeling of HHA, PV system, DVR, and SHLs are all verified using MATLAB\Simulink.

1. Introduction

Voltage quality (VQ) issues in the electricity sector have already been addressed in a number of ways [1], but specialized units like dynamic voltage restorers (DVRs) [2], STATCOM [3], and unified power quality conditioners [4] are particularly useful for enhancing VQ in power distributing networks (PDNs) [5]. Supplying voltage in series by DVR is a suitable tool for mitigating voltage sag (V_S). V_S is primarily brought on by system faults especially short circuits and overloads. Its degree and the employment of an appropriate DVR rely on the system's nature, the fault location, type, and impedance, as well as the protection sort. Utilizing DVR is one of the best ways to augment VQ [2, 6]. Numerous types of specialized units were outlined in references [7, 8] together with their functions and merits. Previously and current control solutions mostly concentrate on the voltage compensation step to lower the DVR's voltage and capacity rating needed. Additionally, phase jump (PJ) correction has drawn increased attention as well [9].

The interline DVR's effectiveness in V_S alleviating was described in reference [10]. In reference [11], DVR was modeled as an effective tool for protecting sensitive loads from extreme V_S and voltage swells (V_W), and also to control and adjust both V_S and V_W based on the injected power. In reference [12], the analysis of V_S and harmonic suppression using DVR was studied, but renewable generators impacts were not considered. The examination of controlling the voltage of important loads under variable and fluctuating system frequency was made by applying DVR [13]. Despite DVR's expensive cost, which prevented widespread deployment, particularly in PDNs, it was regarded as the superior unit in securing PDNs from disturbances [14]. In both DVR and STATCOM, a series of voltage and shunt currents were injected, respectively, into the power system to reduce VQ disturbances, and this work proved that the DVR was a more economical option than STATCOM [15]. In references [12, 16], the DVR system was tested and successfully mitigated the voltage instability, but renewable energy sources were not well thought-out where these sources inject harmonics into the power system. Literature [17] only studied DVR performance in surpassing V_S/V_W, but our work gives a detailed analysis of DVR to solve the expected VQ problems in PDNs at the low voltage level (LVL).

Due to the flexibility, and low price of the PWM method [18], compared to alternative methods used for multilevel inverter (MI) topologies, the two-level converter (2LC) topology is adopted in this work. The switches in 2LC systems are unable to sustain medium voltage (MV); hence, they cannot be used in MV networks. Outcomes demonstrate great performance in this architecture, with program execution being simple and calculations occurring around 1.66 times faster than in previous topologies [19]. Several papers such as [20, 21] used MI in the DVR system to reduce the switching losses, but MI increases the system cost and complexity which reduce the system reliability. Splitting one DC source into many DC sources was a noticeable issue that appears when applying multilevel topologies [22].

The effects of photovoltaic (PV) systems' radiation and temperature fluctuations were taken into account when designing various sorts of PV cells [23] and [24]. By developing the proper links and controls, PV models can be utilized as renewable generators with wind generators. In reference [25], V_S mitigation in the PDN using a simultaneous injection of reactive current\power was reported. In reference [26], the performance of a PI controller (PIC)-based DVR for V_S alleviating was studied. Electricity price, reliability, and enhancing VQ are of essential significance to customers in smart systems. To fulfill customers and provide clean energy, utilities with smart PDNs spend a lot of money. The smart grid's main elements include the smart home (SH). Any SH includes expensive, and electronic devices, where these devices are sensitive to harmonics and instability voltages. In addition SH operation and concepts were fully described in references [27–29].

Conventional PIC gains can be adjusted using a variety of methods such as fuzzy logic, genetic algorithms (GAs), quadratic linear regulators (QLRs), neural networks (NNs), and others. The primary limitations of employing a QLR are that overshoot and steady-state errors cannot be completely eliminated, while the major drawbacks of using a GA are that it needs basic data and difficult computations [30–32]. The use of NNs produces precise responses, a decrease in deviation, and errors, but it has the drawback that it takes training, and the precision of the outcome is dependent on the quantity of training when used to adjust the coefficient of controllers [33]. The system dynamic response fluctuations and overshoot are reduced when the PID controller is used in place of the PIC, but employing it slows down the system response and also introduces noise when the error is changing quickly [34]. The aforementioned techniques can also be used to adjust the PID controller gains. In this study, Harris Hawks algorithm (HHA) is applied because it achieves success in engineering design problems, satellite image segmentation, air pollution forecasting, prediction of slope stability, two-layer foundation soils, and color image multilevel thresholding segmentation [35]. Finally, to clarify the current work's importance and superiority a comparison with previously published papers interested in the VQ research area using DVR is performed in Table 1.

This study examines the effectiveness of DVR with its upgraded control system and its effects on enhancing VQ at LVL in PDNs. The total harmonic distortion (THD) produced at the low voltage bus (LVB) is decreased with DVR based on the HHA-PIC compared to without DVR in normal and abnormal conditions, which is a fast transient response for alleviating VQ issues. This research also applies the suggested technique to a PDN and investigates how well it compensates for V_S and V_W and presents the simulation software's outcomes. Investigating the effectiveness of an HHA-PIC-based DVR in PDN for VQ enhancement under various fault scenarios is the main contribution of this paper. To further demonstrate the advantages of the HHA technique, comparisons between HHA-PIC and Ziegler–Nichols (ZN)-PIC performance in lowering THD at the LVB are made. The outcomes are highly energizing and useful for SH applications.

The rest of this work is structured as follows: The general structure and system elements under study, including DVR, are covered in Section 2, and the PV system is presented at the end of this part. The construction of the proposed DVR control scheme based on the HHA is then presented in Section 3. In addition, the HHA method is introduced in this part. Following that, Section 4 presents the software simulations and outcomes. Section 5 presents the conclusions from the discussions of simulated scenarios.

2. System Description and Modeling

The current work involves connecting the PV for the SH system to an LVB and connecting it to the power grid via a transformer (11 kV/380 V). Figure 1 shows the proposed configuration, which consists of a PV system, SH, power grid, and a DVR with an upgraded control system. Table 2 lists the investigated system parameters.

2.1. DVR System Analysis. To protect sensitive loads, DVR is typically installed on the LVB to which they are linked. Figure 2 depicts the DVR's structural layout. The storage device, DC capacitor, 2LC, low pass filter (LPF), IT, and bypass switch are the DVR parts. In references [43, 44], details of the DVR unit are described. Literature [45] also offered its equivalent circuit, as well as the voltage and power that it injects under different operating conditions.

The DVR's injected voltage (V_{DVR}) is described as follows [46]:

$$V_{\mathrm{DVR}} = V_L + Z_{TH} I_L - V_{TH} = V_L - V_{\mathrm{grid}}, \quad (1)$$

where V_L, Z_{TH}, I_L, and V_{TH} are the desired load voltage, load impedance, load current, and system voltage under fault conditions, respectively.

I_L is clarified in equation (2):

$$I_L = \frac{P_L + jQ_L}{V}. \quad (2)$$

Equation (1) can be rewritten to be equation (3):

$$V^{*}_{\mathrm{DVR}} = V_L^{\angle 0} + Z_{TH}^{L(\beta-\theta)} - V_{TH}^{L\delta}, \quad (3)$$

$$\theta = \tan^{-1}\left(\frac{\theta_L}{P_L}\right). \quad (4)$$

where θ, (α, β, and δ) are load power factor angles, phase-angles of V_{DVR}, Z_{TH}, and V_{TH}.

The DVR's power output can be written as follows:

$$S_{\mathrm{DVR}} = V_{\mathrm{DVR}} I^{*}_{\mathrm{DVR}}. \quad (5)$$

The inverter is a vital part of the DVR system, notably in terms of cost. The DC-link capacitor, IGBT switches, and LC filter have the most impact on its cost, with the rest of the electronics having just minor effects. Additionally, a clamped diode that is not required in a 2LC design is included in the price of a 3LC. As listed in Table 3, we will investigate the costs and contrast the 2LC and 3LC systems with the expected world average market pricing in 2021. This analysis clearly shows that the 2LC of DVR system is 46% less expensive than a 3LC of DVR system. The approximate cost of manufacturing the 2L-DVR system under investigation is 70 $/KVAR, or, on average, $700. To preserve VQ and stability in SHs while achieving high efficiency, this price is appropriate [35].

A fault must be detected by the applied control system, which must also compute and determine the voltage\current needed for balancing, produce trigger pulses for the used 2LC, and inject the necessary voltage\current. The 2LC must make up for voltage distortions brought on by PDNs. The system's inverter injects standard voltages, which are calculated by the 2LC controller. A sinusoidal voltage control method is suggested for controlling the DVR-2LC. To mitigate entire distortions and maintain a steady voltage in this situation, the DVR should be managed. DVR is managed such that its losses are kept to a minimum while the voltage value is normal. To add voltage to the system as soon as V_S is discovered, DVR must respond quickly. The synchronous reference frame method, which also is built on instantaneous supply data, is used to accomplish this [35]. The control system's overall layout is depicted in Figure 3, along with the system parameters.

2.2. PV System. In general, the PV arrangement under consideration uses DC/DC and DC/AC converters to link the PV array to the LVB [47]. As seen in Figure 4, a PV cell is typically represented electrically by a single diode, series resistance (R_S), and parallel resistance (R_p). Figure 4 symbols are as follows: I_d is the diode current, I is the output current, V is the output voltage, I_{ph} is the produced current, G_a is the irradiance from the sunshine, and T_C is the cell temperature.

The PV's concept and model are fully defined in references [20, 48]. To model the solar cell, the subsequent equations between (6)–(9) are used:

$$I = I_{\mathrm{ph}} - I_o\left(e^{q\,(V - I.R_s/aKT)}\right) - \left(\frac{V + IR_s}{R_p}\right), \quad (6)$$

where k is the Boltzmann constant (1.381×10^{-23} J/K), q is the elementary electron charge (1.602×10^{-19} C), V_d is the diode voltage, I_0 is the reverse saturation current of the diode a is the diode quality factor, t is the temperature, and V is the cell voltage.

The PV terminal voltage can be written as follows:

$$V = \frac{akt}{q}\ln\left\{\frac{I_{ph}}{I} + 1\right\}. \quad (7)$$

The R_s can be given by the following expression:

$$R_s = -\frac{\mathrm{d}V}{\mathrm{d}I} - \frac{akT/q}{I_0 * e^{\left(qV_{\mathrm{OC}}/akT\right)}}. \quad (8)$$

The PV output power ($P_{PV}(t)$) is given by the following expression:

$$P_{PV}(t) = N_{PV}(t)\, V_{pV}(t)\, I_{pV}(t), \quad (9)$$

where $N_{PV}(t)$, $V_{pV}(t)$, and $I_{pV}(t)$ are the number of PV cells, PV voltage, and PV current, respectively.

3. Proposed Control Technique

3.1. Design of PIC Using the ZN Method. Because of PIC's straightforward design, inexpensive price, and high stability margin merits, it is frequently utilized in engineering applications. However, PIC tuning is challenging, particularly in nonlinear dynamic systems (power system elements). The considered DVR includes a PWM with a PIC and it is described in equation (10) [49].

Table 1: Comparison with previously published controllers of DVR.

References	Detection system	Applied controller	The simplicity of the DVR structure	THD analysis	Stability analysis (SA)	Studied cases	Program	Main findings
[36]	DQ	PI	✗	✗	✗	Balanced and unbalanced V_S	PSCAD/ EMTDC	i) Safe grid linked (PV-WT) from V_F with SMES and battery-based DVR.
[37]	DQ	PI	✗	✗	✗	V_S and phase jumps (PJs)	MATLAB/ Simulink and HIL	i) Boost the VQ of sensitive loads (SLs) with the optimal DVR application.
[38]	DQ	PI	✗	✗	✗	V_S	MATLAB/ Simulink	i) A new DVR topology (two 3-phase input matrix converters without a capacitor in the DC-link side (DCLS)) was done to alleviate DVR capacity (limited based on restorer energy).
[39]	RMS	PI	✓	✗	✗	V_S and energy self-recovery	MATLAB and HIL	ii) An improved DVR control scheme was suggested to improve the VQ of SLs. ii) Compensation time was improved while correcting the PJ and hurrying the energy recovery of DCLS.
[9]	DQ	PI	✓	✗	✗	Wide range of V_S	Experimental	i) A dual-DC-DVR was performed to mitigate deep V_S. ii) This solution lowers the dc-dc converter's power rating, allowing for substantially smaller energy losses.
[11]	DQ	Hysteresis	✗	✗	✗	Wide range of V_S	MATLAB/ Simulink	i) Improving VQ in PDN with SMES-based DVR and SFCL ii) This strategy locked the instantaneous magnitudes and phase angles of real-time line voltages. iii) The total capital cost of DVR. Was reduced.
[40]	RMS	PI	✓	✓	✗	Balanced and unbalanced V_S	PSCAD/ EMTDC	i) Dual-functional DVR to limit fault current. ii) This scheme successfully operated under short-circuit fault current-limiting and compensation V_F modes.
[41]	RMS	Fuzzy type 1, 2, and PI	✗	✗	✗	V_S and V_W	MATLAB/ Simulink and HIL	i) Voltage compensation was performed with no bulk DC capacitor and no PLL circuit.
[42]	DQ	CS-PI	✓	✗	✗	V_S, V_W, and unbalanced V	Homer software	i) Enhancement of hybrid (fuel cell\WT\ PV\battery) power system. ii) This study was a benefit for sustainable cities and new communities.
Current paper	DQ	HHA-PI	✓	✓	✓	V_S, V_W, V_F, and DLGF	MATLAB/ Simulink	i) Improving the DVR control system with HHA-PIC to enhance VQ under severe events with low THD.

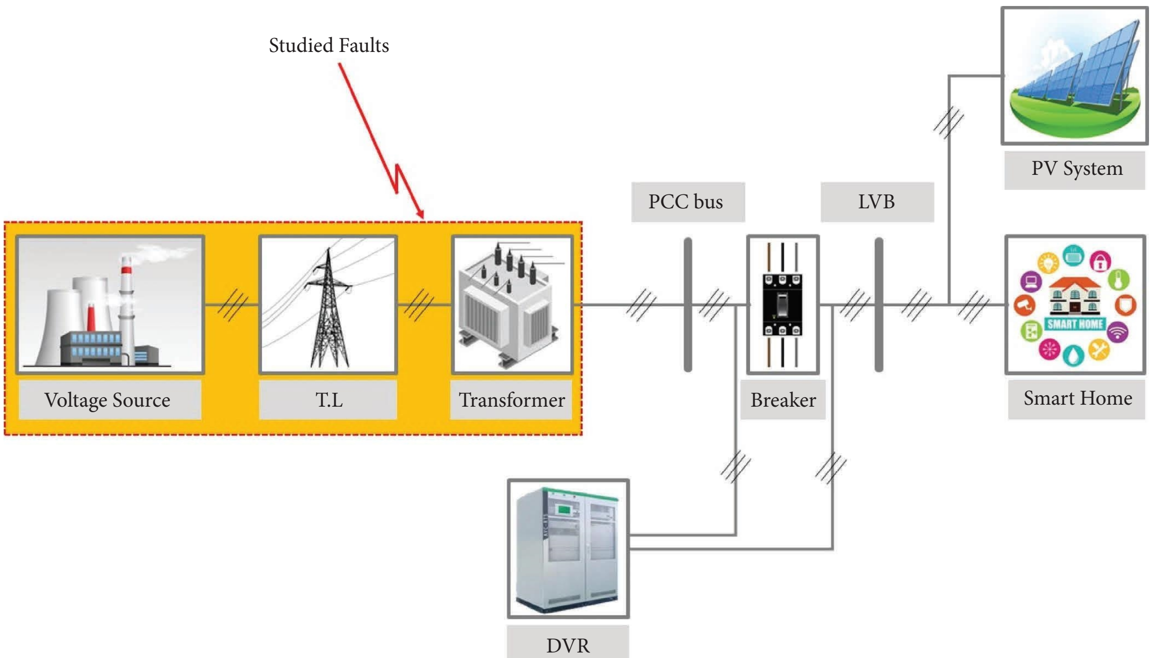

Figure 1: Studied system.

Table 2: Studied system parameters.

Parameters	Value and unit
PCC bus voltage	11 kV
Source impedance	0.001 Ω and 0.1 mH
DVR voltage and LBV	380 V
PV power	20 kW
SH loads	45 kW and 10 kVAR
DVR rating	10 kVAR
DC capacitor size	200 μF
Filter inductance and capacitance size	10 mH and 0.1 μF
Switches type	IGBT
Switching frequency	3000 Hz
Frequency	50 Hz
PV surface temperature	300 K
Number of parallel and series cells	40, and 900
OC voltage of PV	384 V
Radiation range	0–1000 W/m^2
Controller type	PI based on HHA and ZN
Leakage reactance of injection transformer (IT)	UK = 10%
DC source capacity	500 V
IT capacity	3 single-phase 10 KVA
Connection and ratio of IT	Grounded wye/open and 1:1

$$X(t) = K_p\ \varepsilon(t) + K_i \int \varepsilon(t)\mathrm{d}t, \tag{10}$$

where X and ε are functional to the PWM producer and error signal, respectively.

ε is the difference between a desired and injected voltage. Both K_p and K_i values are dependent on system parameters to determine the wanted stability and response. The ZN technique is fully described and discussed for tuning the PIC in references [50, 51].

3.2. HHA Technique. Heuristic optimization algorithms have already been employed to optimize PIC gains. The HHA is a metaheuristic method that imitates the cooperative behavior of the HH's successful pursuit technique. It includes the phases of exploration and exploitation similar to other algorithms. Two exploration phases and four exploitation steps are part of the HHA as described in the below equations. Additionally, a novel stochastic strategy to solve several optimization methods is suggested by the mathematical depiction of this cooperative action. The following

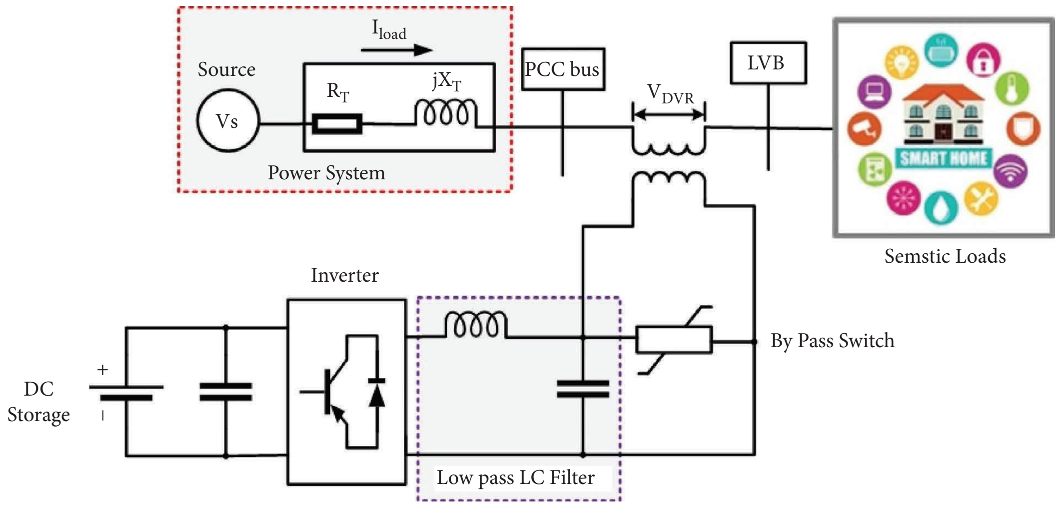

Figure 2: DVR configuration.

Table 3: Cost analysis of two and three-level inverters.

Inverter element	*Unit price ($)*		*No. of units*		*Total unit prices ($)*	
	2L (proposed)	3L	2L (proposed)	3L	2L (proposed)	3L
IGBT	20	20	3	3	60	60
Capacitor	60	60	6	8	360	480
Diode	✗	30	✗	6	✗	180
Total cost ($)					420	720

stages, which are imitated and simulated by the HHA mathematical model, are used by HHs to hunt their rabbits. It is used in this study because, when tested against 29 unrestricted benchmark issues and 6 limited design engineering tasks, it performed better than the other 11 approaches [52]. The following equations are employed to represent the HH's behavior while around rabbits, and the idea of the HHA is completely defined in [52–54]. The implementation of the suggested HHA on the DVR control system is shown in a flowchart in Figure 5.

(1) Exploration phase:

$$Y(t+1) = \begin{cases} Y_{\text{rabit}}(t) - Y_m(t) - C_3\left(LB + C_4(UB - LB)\right), & q < 0.5 \\ Y_{\text{random}}(t) - C_1\left|Y_{\text{random}}(t) - 2C_2 Y(t)\right|, & q \geq 0.5 \end{cases}, \quad (11)$$

$$Y_m(t) = \frac{1}{N}\sum_{i=1}^{N} Y_i(t).$$

(2) The transition from exploration to exploitation:

$$E = E_O\left(1 - \frac{t}{T}\right). \quad (12)$$

(3) Exploitation phase:

(a) Soft besiege, $C \geq 1/2$ and $|E| \geq 1/2$

$$Y(t+1) = \Delta Y(t) - E\left|qY_{\text{rabit}}(t) - Y(t)\right|, \quad (13)$$

where

$$\Delta Y(t) = Y_{\text{rabit}}(t) - Y(t). \quad (14)$$

(b) hard besiege $C \geq 1/2$ and $|E| < 1/2$

$$Y(t+1) = Y_{\text{rabit}}(t) - E|\Delta Y(t)|. \quad (15)$$

(c) soft besiege with progressive rapid dives $C < 1/2$ and $|E| \geq 1/2$

$$H = Y_{\text{rabit}}(t) - E\left|qY_{\text{rabit}}(t) - Y(t)\right|,$$

$$G = H + 0.01\,S\,\frac{u\,\sigma}{|\gamma|^{1/\beta}}, \quad (16)$$

where,

$$\sigma = \left(\frac{\Gamma(1+\beta)\sin((\pi\beta)/2)}{\Gamma((1+\beta)/2)\beta\, 2^{((\beta-1)/2)}}\right)^{1/\beta}. \quad (17)$$

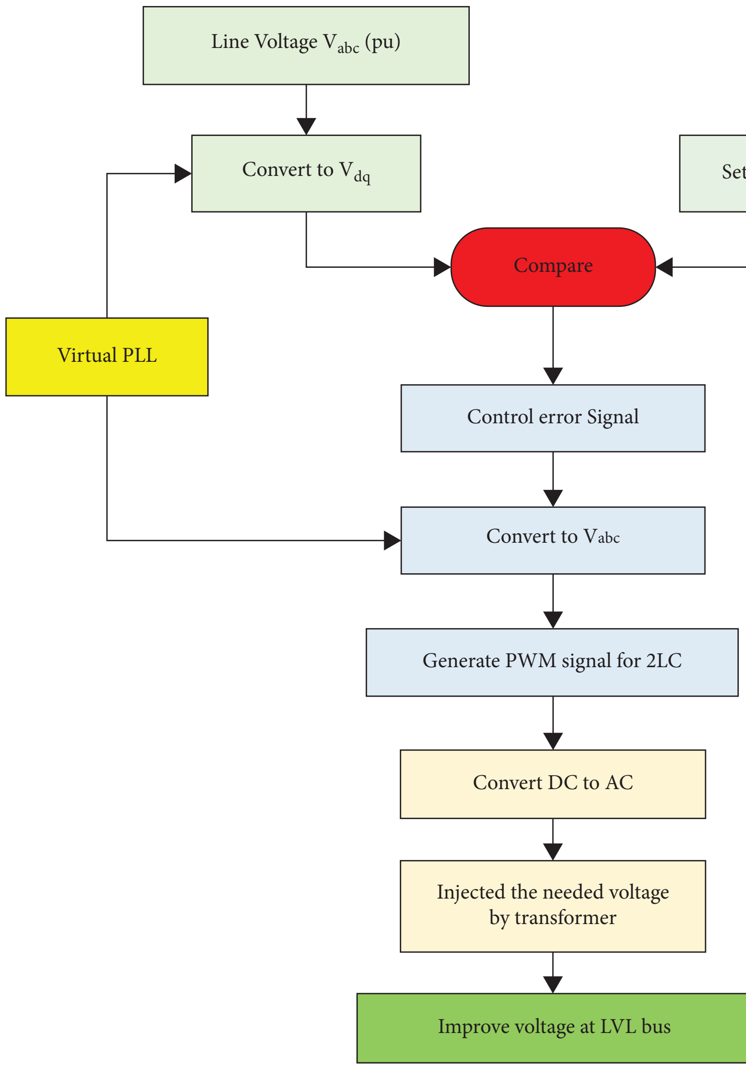

Figure 3: DVR control strategy.

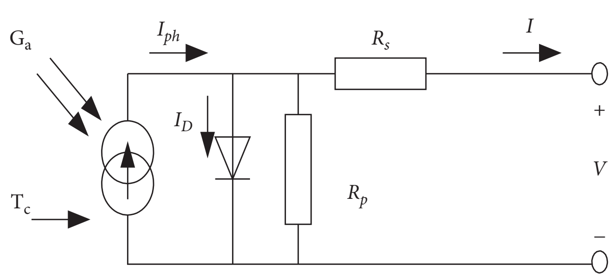

Figure 4: Equivalent circuit of a solar cell.

(d) hard besiege with progressive rapid dives $C < 1/2$ and $|E| < 1/2$

$$Y(t+1) = \begin{cases} \Delta H & \text{if } F(H) < F(Y(t)) \\ \Delta G & \text{if } F(G) < F(Y(t)) \end{cases}. \tag{18}$$

To choose the optimum PIC parameters, HHA and the ZN technique are contrasted in this study. The objective function provided by equation (19) to minimize the integral time absolute error (ITAE) serves as the foundation for the problem formulation for the DVR control system. The chosen PIC gains for the investigated options are presented in Table 4.

$$\mathrm{ITAE}_{d\backslash q} = \int_0^{\infty} t \left| e_{vl\ d\backslash vlq} \right| dt. \tag{19}$$

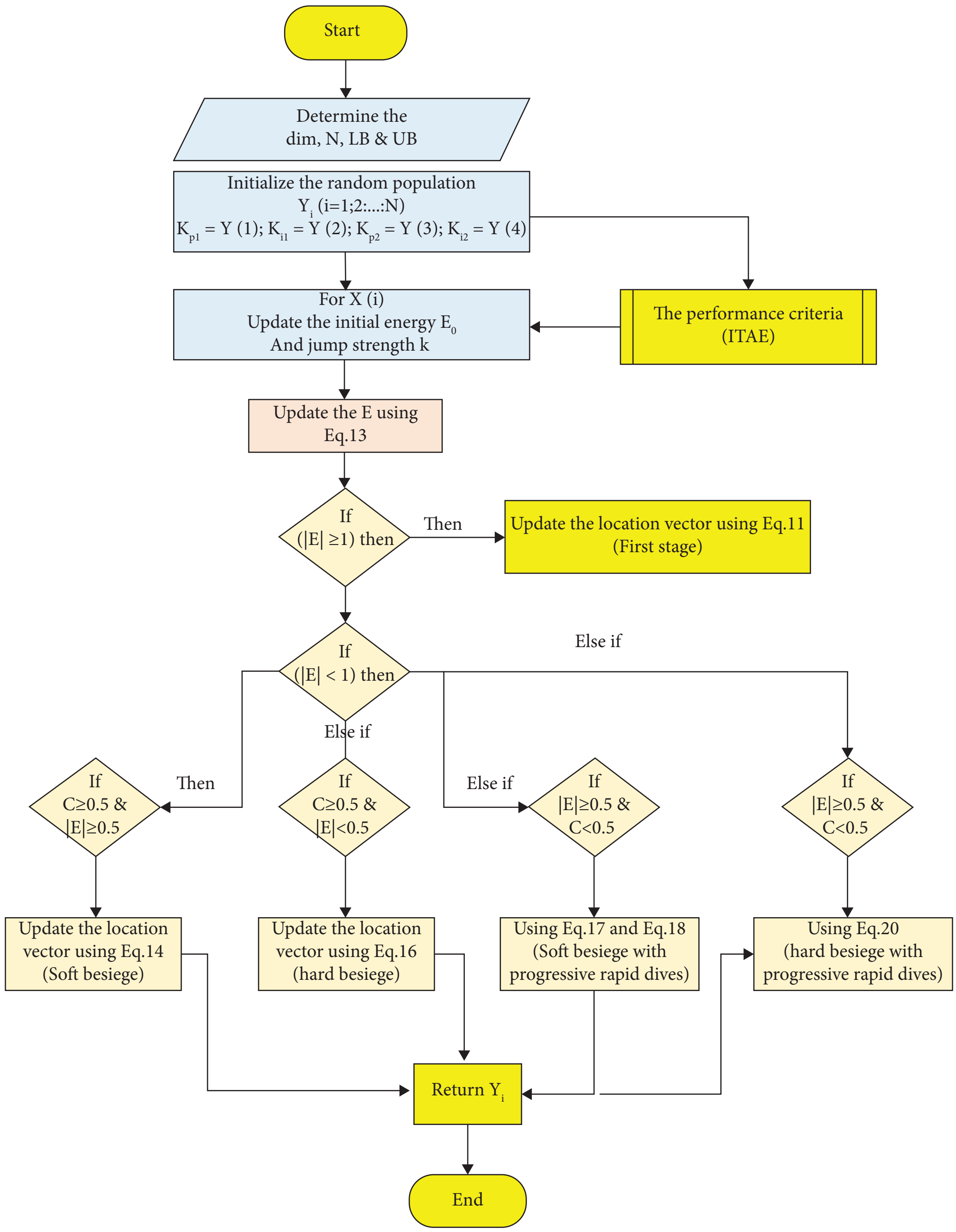

Figure 5: HHA flowchart.

3.3. Proposed HHA-PIC. The proposed DVR control system operation is depicted in Figure 6. V_{abc} at the PCC are transformed to the $V_{\alpha\beta}$ and then to the V_{dq} using Clark's transformation. V_{PCCd} is compared with its reference value to produce the error (e_{PCCd}) and then e_{PCCd} is passed through a rate limiter to regulate its impact on the reaction of the control scheme reaction to eliminate load voltage (V_L) overshoot. At the same time, the direct V_L (V_{Ld}) is compared with its reference value to produce the error (e_{VLd}) and then e_{VLd} is conditioned using the PIC_1 to produce e_{CVLd}. The e_{CVLd} is summed up with e_{PCCd} to produce e_{Cd}. Meanwhile, the quadrature V_L (V_{Lq}) is compared with its reference value to produce the error (e_{VLq}); then, e_{VLq} is conditioned via the PIC2 to generate e_{Cq}. Both e_{Cd} and e_{Cq} are transformed back to $V_{\alpha\beta}$ employed to generate the appropriate space vector

Table 4: Obtained PIC gains using HHA and ZN techniques.

Technique	Obtained PI gains			
	K_{p1}	K_{p2}	K_{i1}	K_{i2}
ZN-PI	0.7213	0.9287	39.3651	5.23713
HHA-PI (proposed)	1.0926	3.1941	69.9031	19.1764

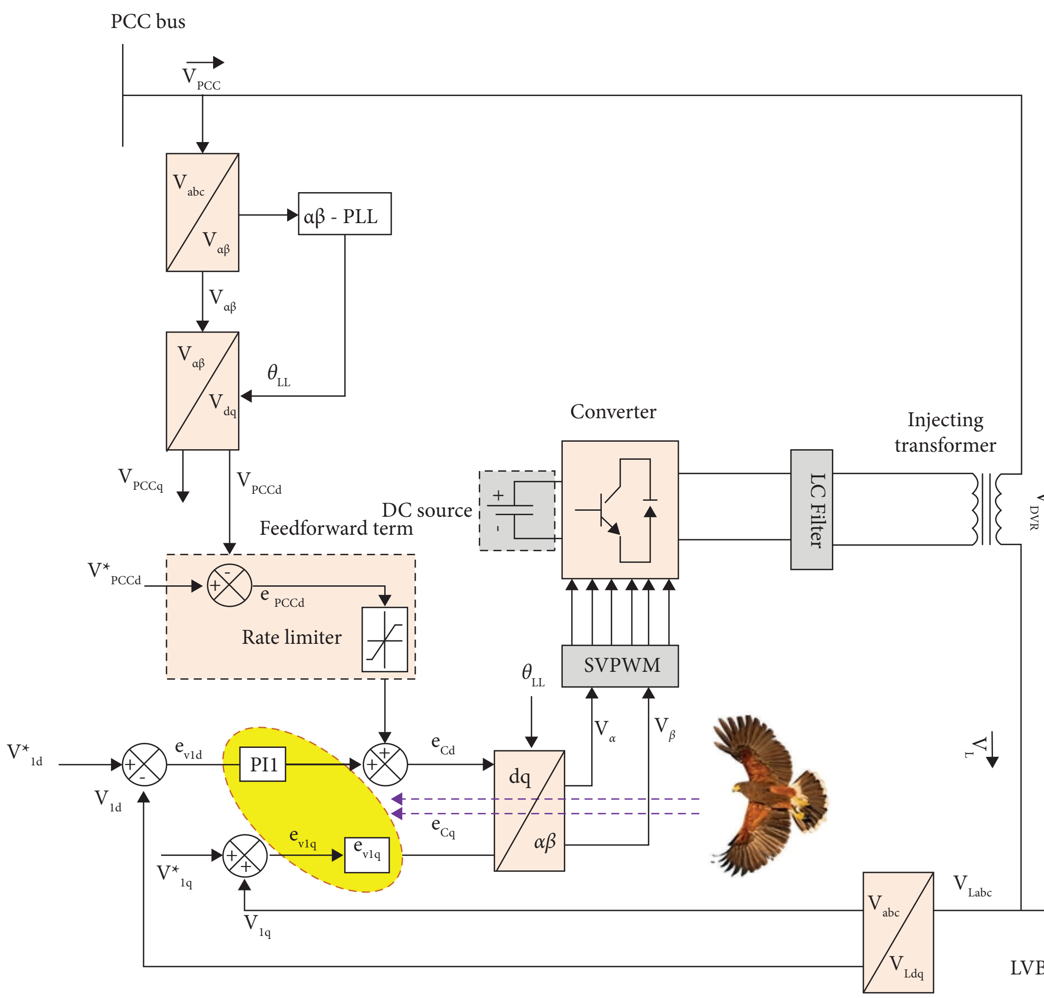

Figure 6: DVR proposed control system-based HHA-PIC.

PWM signal. This signal is used to control the converter switches. The converter output voltage is stepped down with the series IT to the electric grid voltage level to get the V_{DVR}. V_{DVR} is summed up with V_{PCC} to produce the regulated V_L. During the compensation process, the feedforward term and the closed-loop feedback control signal are combined to improve the transient responsiveness and get rid of unwanted transient oscillation as seen in Figure 6.

3.4. Analysis of the System's Robustness and Stability. Many theories, including the Bode diagram, zero pole mapping, and Lyapunov function (LF), can be used to evaluate SA [55, 56]. LF is taken into consideration because it has demonstrated its efficacy in several engineering issues [57]. Equation (1) illustrates the fundamental idea of the DVR, in which the suggested controller will calculate and adjust for all upsets and uncertainties instantaneously while detecting the system's standard voltage, or LPF. An LPF $G_\nu(s)$ is in this research to facilitate the suggested controller layout. As a first-order filter, $G_\nu(s)$ has indeed been chosen, where, $G_\nu(s) = 1/(1+\tau_\nu)$.

Also, V_L in (1) can be expressed as follows:

$$V_L = L^{-1}\left\{\frac{1}{1+\tau_\nu}\right\} * \left(V_{\text{grid}} + V_{DV\,R}\right), \qquad (20)$$

where the symbols τ_ν, L^{-1}, $*$ are the time constant, inverse Laplace transformation, and convolution operator, respectively.

Equation (20) is a representation of the dynamics:

$$\dot{V}_L = \frac{V_{DVR}}{\tau_\nu} + \Delta_\nu, \qquad (21)$$

where $\Delta_\nu = -(V_L/\tau_\nu) + (V_{\text{grid}}/\tau_\nu)$, and the symbol Δ_ν represents the lumped uncertain term.

Figure 7 shows the organizational layout of the suggested DVR control system. The standard V_L that the controller uses is produced with normal amplitude, and the frequency and phase are synchronized with the V_{grid} using 3-PLLs [58].

The suggested controller has two inputs (V_L and V_{grid}) and one output (V_{DVR} reference). The voltage control loop includes the inputs. The output is utilized to drive the PWM, which creates the converter's switching signals. A reliable linear reference model should be used in conjunction with the investigated control method to ensure that the closed-

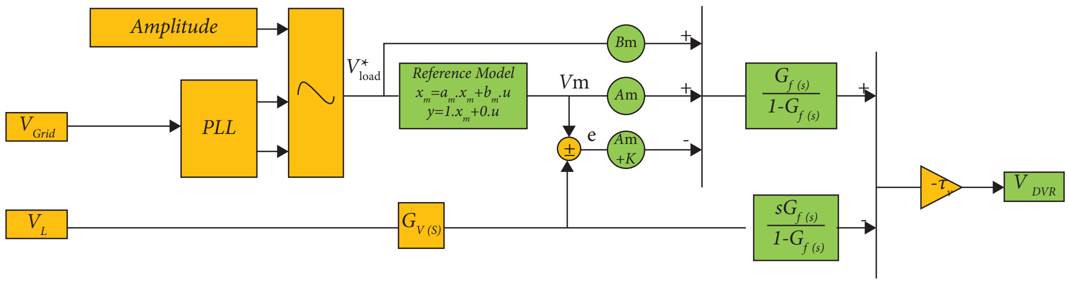

FIGURE 7: Suggested DVR control scheme for SA.

loop system responds as needed [59]. The following can be expressed as the V_{DVR} control signal:

$$V_{DVR} = \tau_v \left(A_m v_m + B_m V_L^*\right) - \tau_v \left(A_m + K\right) e(t) - \tau_v \left[L^{-1}\left\{G_f(t)\right\} * \left(\dot{V}_L - \frac{V_{DVR}}{\tau_v}\right)\right]. \tag{22}$$

Using the process outlined in reference [60] supports assessing the LF bounds for V_L. The controlled system's SA has been implemented using the LF below.

$$V(t) = V_L V_L^T. \tag{23}$$

With derivation of (23) and given V_L dynamics (21) and V_{DVR} (22), the SA is executed as follows:

$$\begin{aligned}
\dot{V}(t) &= \dot{V}_L^T V_L + V_L^T \dot{V}_L = \left(\frac{V_{DVR}^T}{\tau_v} + \Delta_v^T\right) V_L + V_L^T\left(\frac{V_{DVR}}{\tau_v} + \Delta_v\right) \\
&= V_L\left\{V_m^T A_m^T + (V_L^*)^T B_m^T\right\} - V_L\left\{\left(V_m^T - V_L^T\right)\left(A_m^T + K^T\right)\right\} + V_L\left\{\Delta_v^T - L^{-1}\left\{G_f(t)\right\} * \left(\Delta_v^T\right)\right\} \\
&\quad + V_L^T\left\{A_m V_m + B_m V_L^*\right\} - V_L^T\left\{(A_m + K)(V_m - V_L)\right\} + V_L^T\left\{\Delta_v - L^{-1}\left\{G_f(t)\right\} * (\Delta_v)\right\} \\
&= V_L\left\{(V_L^*)^T B_m^T - V_m^T K^T\right\} + V_L\left\{V_L^T\left(A_m^T + K^T\right)\right\} + V_L\left\{L^{-1}\left\{1 - G_f(t)\right\} * \left(\Delta_v^T\right)\right\} \\
&\quad + V_L^T\left\{B_m V_L^* - K V_m + (A_m + K) V_L\right\} + V_L^T\left\{L^{-1}\left\{1 - G_f(t)\right\} * (\Delta_v)\right\} \\
\dot{V}(t) &= V_L^T\left(A_m^T + K^T + A_m + K\right) V_L + (V_L^*)^T B_m^T V_L + V_L^T B_m V_L^* - V_m^T K^T V_L - V_L^T K V_m \\
&\quad + L^{-1}\left\{1 - G_f(t)\right\} * \left(\Delta_v^T V_L + V_L^T \Delta_v\right).
\end{aligned} \tag{24}$$

When $= A_m{}^T + K^T + A_m + K$, the equation is formulated as follows:

$$\begin{aligned}
\dot{V}(t) &\leq \lambda_{\max}(Q) V_L^2 + 2B_m V_L^* V_L + 2K V_m V_L + L^{-1}\left\{1 - G_f(t)\right\} * \left(\frac{2V_L^2}{\tau_v}\right) + L^{-1}\left\{1 - G_f(t)\right\} * \left(\frac{2V_L V_{\text{grid}}}{\tau_v}\right) \\
&= L^{-1}\left\{\lambda_{\max}(Q) + \frac{2}{\tau_v} - \frac{2}{\tau_v} G_f(t)\right\} * V_L^2 + 2B_m V_L^* V_L + 2K V_m V_L + L^{-1}\left\{1 - G_f(t)\right\} * \left(\frac{2V_L V_{grid}}{\tau_v}\right),
\end{aligned} \tag{25}$$

where Q is the nonpositive semi-fixed with the Hurwitz matrix $(A_m + K), \lambda_{\max}(Q) <$ zero, and is the supreme eigenvalue of Q. $\zeta = 2B_m V_L^* + 2K V_m + L^{-1}\left\{1 - G_f(t)\right\} * (2V_{\text{grid}}/\tau_v)$ is a limited signal with the upper limit of P, where p is a positive number.

$$\dot{V}(t) \leq \left(\lambda_{\max}(Q) + \frac{2}{\tau_v}\right) V_L^2 + 2\zeta V_L. \tag{26}$$

When Young's inequality is applied,

$$\dot{V}(t) \leq \left[\lambda_{\max}(Q) + \frac{2}{\tau_{v}} + \varepsilon^{2}\right]V_{L}^{2} + \frac{\zeta^{2}}{\varepsilon^{2}} \leq -\lambda_{1}V(t) + \lambda_{2}, \quad (27)$$

where $\lambda_1 = [\lambda_{\max}(Q) + 2/\tau_v + \varepsilon^2], \lambda_2 = p/\varepsilon^2$ and is a tuning coefficient to calculate λ_2 size.

Using $\lambda_1 >$ zero yields the correct design for the error signal feedback gain $(A_m + K)$. Therefore, equation (28) is expressed as follows:

$$0 \leq V(t) \leq V(0)e^{-\lambda_1 t} + \frac{\lambda_2}{\lambda_1}\left(1 - e^{-\lambda_1 t}\right). \quad (28)$$

When $t \longrightarrow \infty$, $e^{-\lambda_1 t}$ tends to 0 makings $V(t)$ in (28) upper limited by λ_2/λ_1. As a result, for all $t \geq 0$, $V(t)$ has no upper and lower bounds. According to the study above, the closed-loop system is stable with respect to LF bounds.

4. Simulated Results and Discussion

Numerous delicate electrical and electronic parts of SHs, such as nonlinear loads fed by renewable energy sources like PV systems, can rise harmonics and VQ disturbances at the LVB where these systems are connected. Figure 1 shows the single-line schematic of the studied configuration. In this part, to verify the effectiveness of the DVR control system optimized by the HHA in mitigating VQ disturbances, a set of simulation scenarios have been carried out using MATLAB/Simulink environment within a changeable voltage profile in the grid. For more details, the system characteristics (PV, SH, DVR, and other elements) used in the simulation process are listed in Table 2. The studied simulation scenarios are: V_S, V_W, voltage fluctuations (V_F), and transient double line to ground fault (DLGF) as well as measuring generated harmonics at the LVB are performed to assess the DVR efficacy. The HHA is designed and implemented in the DVR two-control loop system to obtain the optimal PIC gains, which improves the functionality of the DVR. Additionally, as shown in Table 5, %THD at LVB is assessed in the investigated scenarios to further elucidate the efficacy of the HHA. To properly validate the DVR impact on VQ improvement, the security mechanisms are turned off in the current article during fault situations.

4.1. Scenario A: $\mathbf{V_S}$ *Alleviation.* A serious fault that happens at the grid leads to 54% V_S at the LVB for (0.04–0.06) seconds, as depicted in Figure 8(a). Figure 8(a) and 8(b) depicts the waveforms of the 3-phase voltage at the LVB without and with improved DVR control loops, respectively. Injection of the proper voltage value by DVR maintains the voltage at LVB at its rated value of 1 pu, which reflects the DVR role. The installation of the DVR system quickly restored the value of V_S in 0.5 ms as depicted in Figure 8(b).

The injection voltage from the DVR is not completely sinusoidal because it is dependent on PWM and higher frequency switches, and this issue makes harmonics arise\ appearance. To boost the DVR's dynamic performance, it is therefore required to upgrade the control system. Equation (29) yields the value of %THD of the voltage (THD_V) [61].

$$\%THD_V = \frac{\sqrt{\sum_{h=2}^{h=n} V_h}}{V_1} \times 100\%, \quad (29)$$

where V_1 and V_h are voltage fundamental and voltage harmonic components, respectively.

The obtained %THD of voltages in the studied operating conditions: without DVR\base case (OC_1), ZN-PIC-based DVR (OC_2), and HHA-PIC-based DVR (OC_3) are 17.19%, 3.9%, and 1.74%, respectively at the LVB as listed in Table 5. THD reduction in OC_3 was 89.877%, compared to 77.31% in OC_2, showing a significant improvement in these waveforms and the significance of the HHA.

4.2. Scenario B: V_W *Alleviation.* A severe fault that takes place at the grid results in 160% V_W during the range, $t = 0.04$ seconds and $t = 0.06$ seconds, as shown in Figure 9(a). Figure 9(a) and 9(b) displays the waveforms of the 3-phase instantaneous voltage at the LVB either without or with an upgraded DVR control system, respectively. The voltage at LVB is kept constant at 1 pu by infusing the desired voltage value by the DVR unit fast (0.5 ms), as shown in Figure 9(b). Additionally, maintaining the voltage at 1 pu ensures that the devolved DVR equipment properly does its necessary work (mitigation of V_W).

The measured %THD of voltages in OC_1, OC_2, and OC_3 are 14.97%, 2.04%, and 1.28%, respectively, at the LVB during V_W as listed in Table 5. In OC_2, THD percentage reduction was 86.37%, while THD percentage reduction in OC_3 was 91.38% showing a significant improvement in these waveforms and the value of the HHA. As a result, in both these instances (V_W scenario) and the one before it (V_S scenario), using an HHA-PIC in the DVR control loops is preferable to using a ZN-PIC.

4.3. Scenario C: $\mathbf{V_F}$ *Alleviation.* In this scenario, the dynamic performance assessment of devolved DVR to surpasses V_F is investigated here. The system voltage fluctuated between 0.04 and 0.08 seconds, V_W reaches 1.5 pu from (0.06–0.08 seconds) and V_S reaches 0.65 pu from (0.04–0.06 seconds) as displayed in Figure 10(a). Figure 10(a) and 10(b) depicts the waveforms of the 3-phase voltages at the LVB either without or with an upgraded DVR control system, respectively. Figure 10(b) illustrates that the proposed DVR successfully surpasses the harsh fluctuated voltage and kept it at its reference value (1 pu).

The generated %THD of voltages in OC_1, OC_2, and OC_3 are 29.83%, 5.96%, and 2.76%, respectively, at the LVB during V_F as listed in Table 5. In OC_2, THD percentage reduction was 80.02%, while THD percentage reduction in OC_3 was 90.74% showing an important perfection in voltage waveforms and the HHA effect. From this table, the HHA-PIC performs better than the ZN-PIC for the DVR.

4.4. Scenario D: Mitigation of Transient DLGF. A transient DLGF is applied between (0.03–0.08) seconds at the grid as seen in Figure 11, which causes system instability. Waveforms of 3-phase instantaneous voltage on the LVB with and

Table 5: %THD of voltage for conventional and proposed controllers.

Scenarios	%THD		
	OC_1	OC_2	OC_3 (proposed)
NOC	13.42	0.1	0.04
V_S	17.19	3.9	1.74
V_W	14.97	2.04	1.28
V_F	29.83	5.96	2.76
DLGF	20.79	1.84	1.29

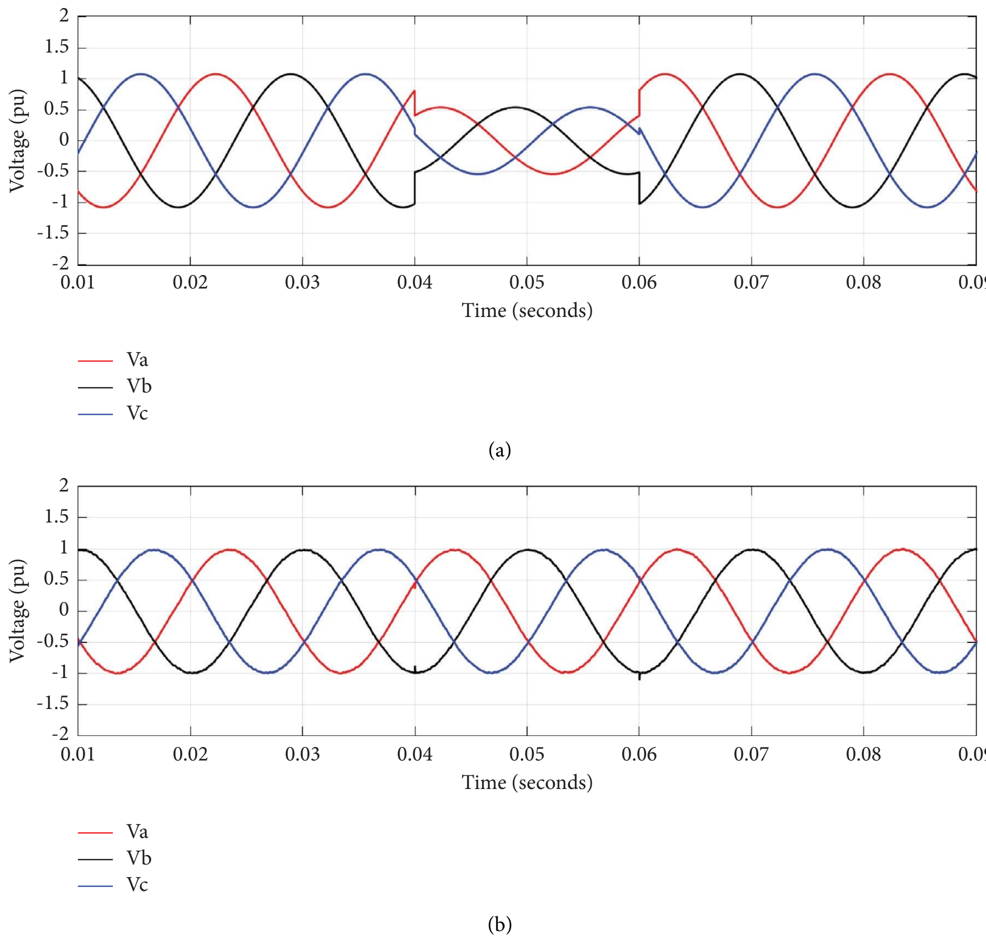

Figure 8: System voltage at LVB under V_S takes place in the grid: (a) without DVR and (b) with improved DVR.

without the proposed DVR are shown in Figure 11(a) and 11(b), respectively. When this fault takes place in the investigated system, the LVB magnitude is decreased from 100% to approximately 40% and that causes voltage instability as seen in Figure 11(a). Figure 11(b) indicates that the DVR overcomes this fault, keeping LVB voltage value at 1 pu, and maintains network stability speedily within 0.5 ms.

The obtained %THD of voltages in OC_1, OC_2, and OC_3 are 20.79%, 1.84%, and 1.29%, respectively, at the LVB under DLGF as listed in Table 5. In OC_2, THD percentage reduction was 91.14%, while THD percentage reduction in OC_3 was 93.79% which indicates a great enhancement in these waveforms and the HHA importance. Consequently, in this scenario, the same as in previous scenarios, the use of an HHA-PIC in the DVR control loops is superior to the ZN-PIC. Table 6 sums up voltage values under all studied fault scenarios for clarifying the benefit and impact of the developed DVR.

4.5. Harmonics Mitigation Analysis. The main reasons for generated harmonics are power converters and nonlinear loads, discharge lighting, and electrical machinery. THD thus appears as one of the key factors to consider when examining the output waveforms of an electric system. The voltage harmonics have reached high hazardous levels at the LVB under regular conditions, exceeding the allowable limits, and exposing the LVB elements to severe damage. The

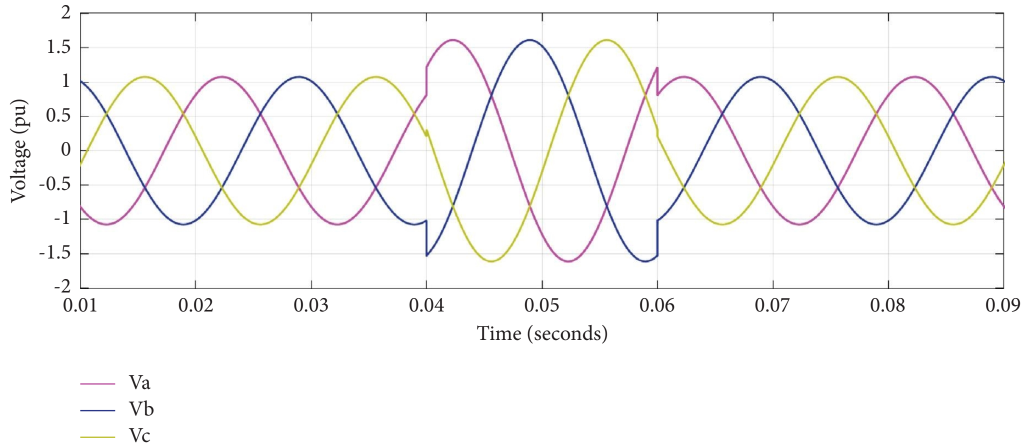

(a)

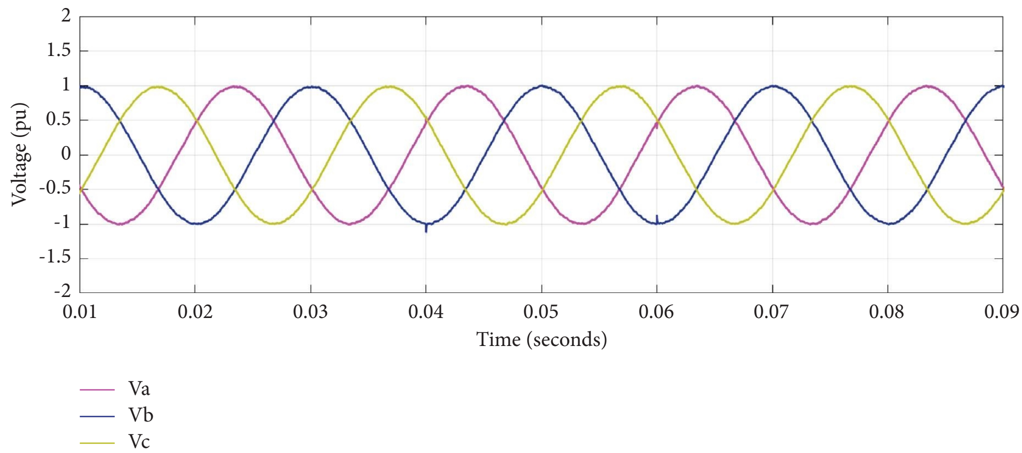

(b)

Figure 9: System voltage at LVB under V_W takes place in the grid: (a) without DVR and (b) with improved DVR.

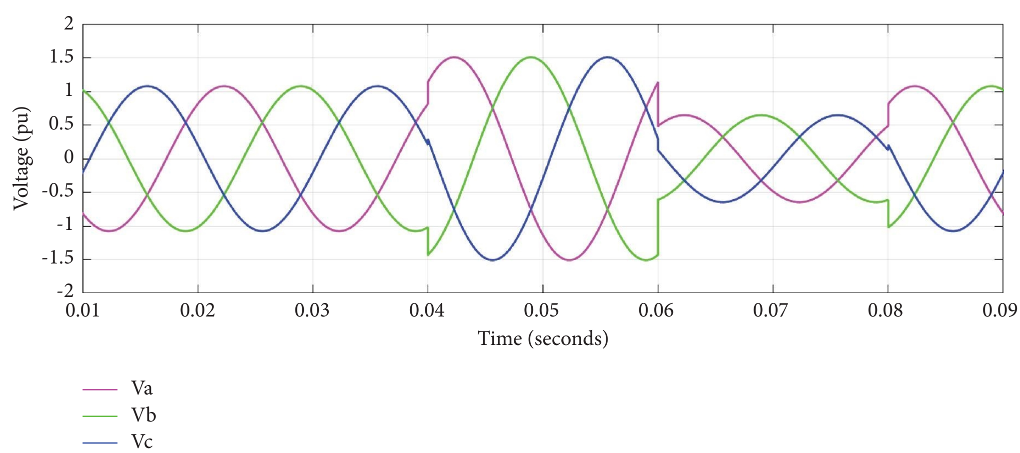

(a)

Figure 10: Continued.

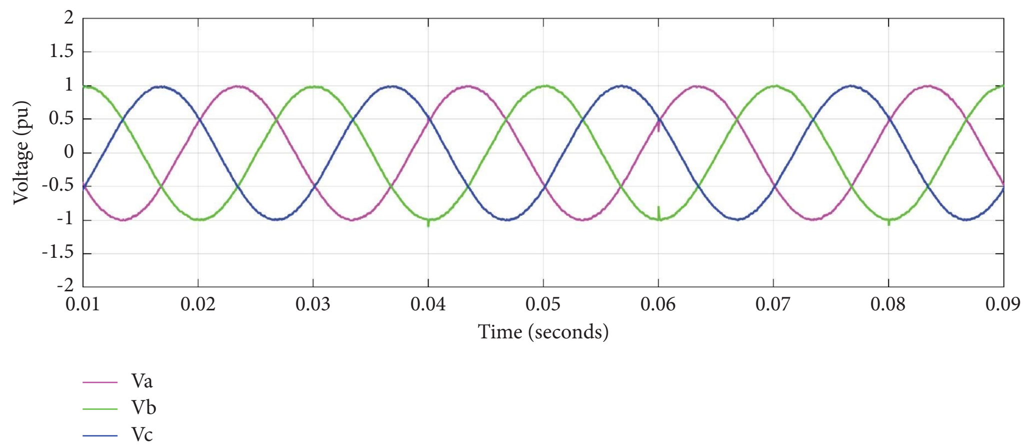

(b)

Figure 10: System voltage at LVB under V_F happens in the grid: (a) without DVR and (b) with improved DVR.

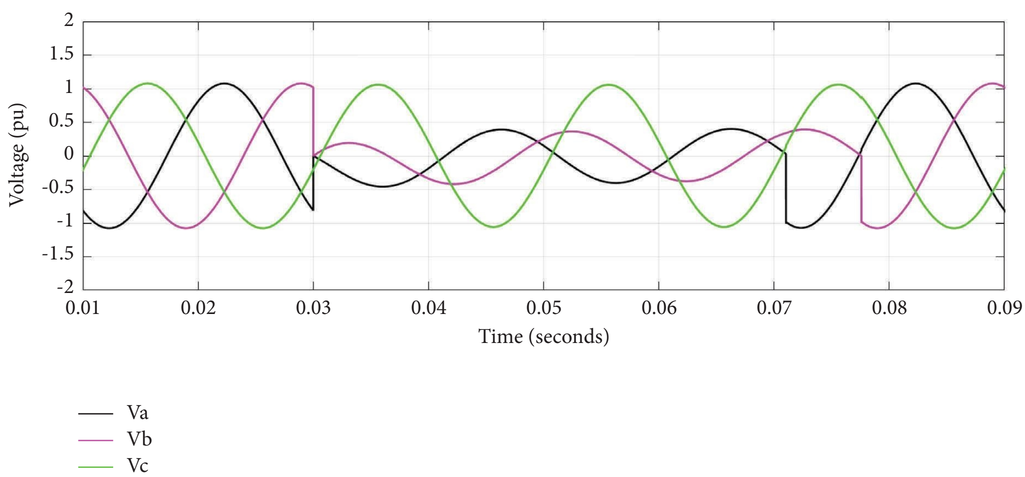

(a)

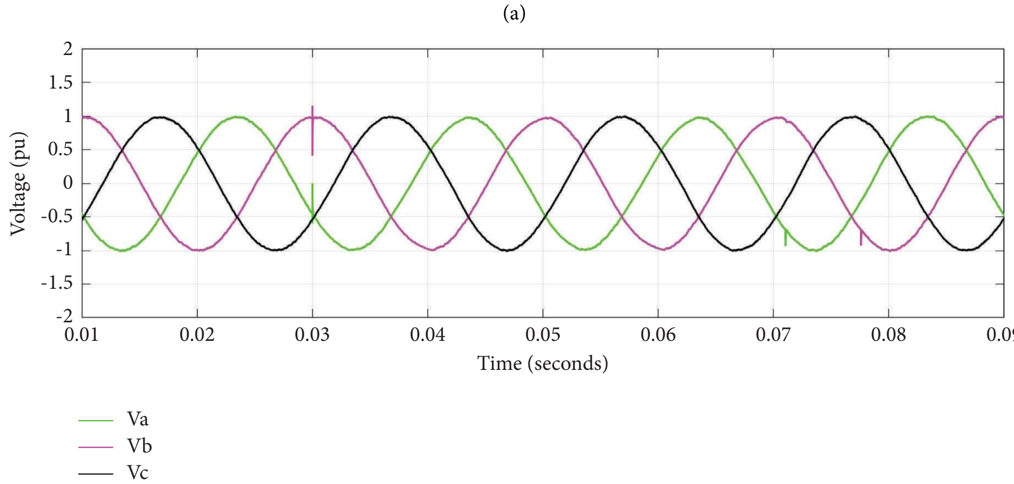

(b)

Figure 11: System voltage at LVB under DLGF occurs in the grid: (a) without DVR and (b) with improved DVR.

obtained %THD of voltages in OC_1, OC_2, and OC_3 are 13.42%, 0.1%, and 0.04%, respectively, at the LVB during normal operating condition (NOC) as listed in Table 6. In OC_2, THD percentage reduction was 99.25%, while THD percentage reduction in OC_3 was 99.71% which indicates a great enhancement in these waveforms and the HHA method impact.

Table 6: Performance comparison of LVB values during studied scenarios.

Studied scenarios	Voltage values under presented configurations (pu)		Period (seconds)
	OC_1	OC_3 (Proposed)	
V_S	0.54	1	0.02
V_W	1.6	1	0.02
V_F	0.65 and 1.5	1	0.04
DLGF	0.4	≈1	0.05

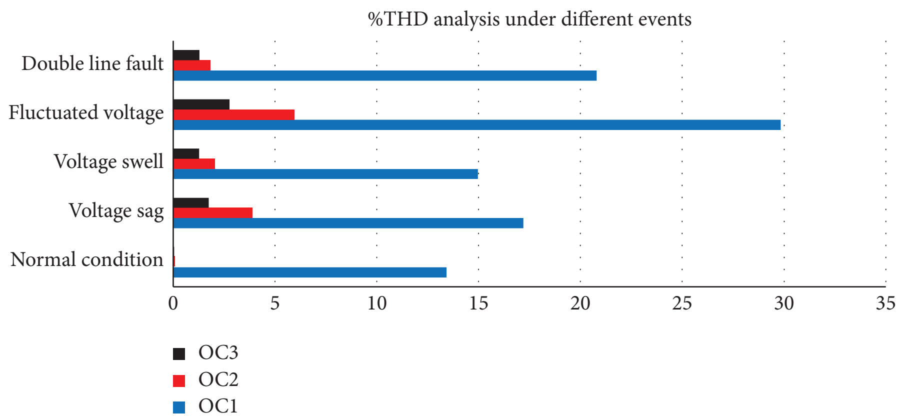

Figure 12: Performance comparison of OC_1, OC_2, and OC_3 under investigated scenarios.

The %THD results are clarified in Table 6, which involve normal and abnormal operating conditions. Table 5 indicates the superiority of the HHA-PIC over the conventional ZN-PIC in mitigating harmonics. In addition, more instability in the system voltage injects more harmonics. The bar chart in Figure 12 is used to display the performance comparison of all OC_1, OC_2, and OC_3 in terms of percentage figures for %THD of LVB to highlight the superiority of the HHA-PIC for the DVR. In particular, it is useful for showing the relationship between OC_1, OC_2, and OC_3 and % THD under the studied scenarios.

5. Conclusion

This manuscript proposed an optimized and efficient DVR control system to effectively protect LVB from voltage abnormalities with low THD. The PICs of DVR are designed and implemented using the proposed HHA and ZN methods to mitigate the studied harsh operating events that may take place in the power system. To emphasize the distinctive contribution of this work, a review of other pertinent previous publications on the subject has also been summarized and presented. The analysis and validation of the suggested controller's stability using LF stability show that the control has been bounded stable. The outcomes prove that HHA is efficiently finding the optimal PIC gains with no complexity and simple calculations. Furthermore, the obtained gains from HHA compared to ZN showed that the DVR was more efficient, especially in reducing harmonics. The efficiency of the proposed approach OC_3 is assessed under V_S, V_W, V_F, and DLGF scenarios and it improves the VQ as well as harmonics reduction compared with OC_2 and OC_1. Tables 5 and 6 show the voltage values and %THD of voltage, respectively, at LVB under all the studied scenarios to declare the effectiveness of HHA. Performance-wise, HHA-PIC outperforms ZN-PIC, and THD generated by DVRs based on HHA-PIC is lower than THD produced by DVRs based on ZN-PIC. The THD study revealed that V_F was the worst scenario, and with ZN-PIC %THD damped by 80.02%, this percentage was insufficient to keep the LVB within acceptable bounds (per IEEE standards), whereas HHA-PIC %THD damped by 90.74%, was sufficient to do so. Finally, it can be mentioned that with OC_3, simple control method, faster response, balanced voltages, and effective harmonic cancelation are the deduced key points that assist SH to operate without VQ problems.

5.1. Future Research Directions. The future research directions of the current study are as follows:

(1) Adaption of the optimized DVR controller with HHA for microgrids applications
(2) Integration of fuel cell at the DC side of DVR and comparing it with battery and PV systems
(3) Implementing newly hybrid optimization algorithms
(4) The proposed option can be applied to achieve fault ride-through capability for renewable generators

Abbreviations

DVR: Dynamic voltage resistor
THD: Total harmonic distortion
VQ: Voltage quality
PWM: Pulse-width modulation
V_W: Voltage swell

V_S: Voltage sag
PDNs: Power distributing networks
2LC: Two-level converter
MV: Medium voltage
PCC: Point of common coupling
LVB: Low voltage bus
LVL: Low voltage level
PIC: PI controller
GA: Genetic algorithm
QLR: Quadratic linear regulator
NNs: Neural networks
ZN: Ziegler–Nichol's
HHA: Harris Hawks algorithm
DLGF: Double line to ground fault
SH: Smart home
IEEE: Institute of Electrical and Electronics Engineers
V_F: Voltage fluctuations
MI: Multilevel inverter
IT: Injection transformer
PV: Photovoltaic
NOC: Normal operating condition
CS: Cuckoo Search
HIL: Hardware-in-the-loop
PSCAD: Power system computer-aided design
EMTDC: Electromagnetic transient design and control
OC_1: Without DVR\base case
OC_2: ZN-PIC-based DVR
OC_3: HHA-PIC-based DVR
pu: per unit.

Data Availability

The data used to support the findings of the study are available on request from the corresponding author.

Conflicts of Interest

The authors declare that they have no conflicts of interest regarding the publication of this article.

References

[1] V. Blazek, M. Petruzela, T. Vantuch, Z. Slanina, M. Stanislav, and W. Walendziuk, "The estimation of the influence of household appliances on the power quality in a microgrid system," *Energies*, vol. 13, no. 17, p. 4323, 2022.
[2] B. Mohit, "Design and simulation of hybrid DG system fed single-phase dynamic voltage restorer for smart grid application," *Smart Science*, vol. 8, no. 1, pp. 24–38, 2020.
[3] P. A. M. Pramila, "DSTATCOM performance for voltage sag swell mitigation," *International Journal of Recent Technology and Engineering*, vol. 9, no. 2, pp. 71–74, 2020.
[4] M. Dashtdar, M. Bajaj, S. M. Hosseinimoghadam, and B. S. Rehman Goud, "Improving voltage profile and reducing power losses based on reconfiguration and optimal placement of UPQC in the network by considering system reliability indices," *International Transactions on Electrical Energy Systems*, vol. 31, no. 11, Article ID e13120, 2021.
[5] M. M. Mahmoud, M. M. Aly, and A.-M. M. Abdel-Rahim, "Enhancing the dynamic performance of a wind-driven PMSG implementing different optimization techniques," *SN Applied Sciences*, vol. 2, no. 4, Article ID 684, 2020.
[6] M. Singh and A. K. Singh, "A single index for voltage quality ranking in the distribution power networks using multiple criteria decision-making," *International Transactions on Electrical Energy Systems*, vol. 31, no. 8, 2021.
[7] M. Bajaj and A. K. Singh, "Grid integrated renewable DG systems: a review of power quality challenges and state of the art mitigation techniques," *International Journal of Energy Research*, vol. 44, no. 1, pp. 26–69, 2020.
[8] M. M. Mahmoud, M. Khalid Ratib, M. M. Aly, and A. M. M. Abdel-Rahim, "Wind-driven permanent magnet synchronous generators connected to a power grid: existing perspective and future aspects," *Wind Engineering*, vol. 46, no. 1, pp. 189–199, 2021.
[9] J. Wang, Y. Xing, H. Wu, and T. Yang, "A novel dual-DC-port dynamic voltage restorer with reduced-rating integrated DC-DC converter for wide-range voltage sag compensation," *IEEE Transactions on Power Electronics*, vol. 34, no. 8, pp. 7437–7449, 2019.
[10] M. Singh and A. k. Singh, "Designing of a solar energy based single phase dynamic voltage restorer using fuzzy logic controlled novel boost inverter," in *Proceedings of the 2020 IEEE 9th Power India International Conference (PIICON)*, pp. 1–6, Sonepat, India, 2020.
[11] Z. Zheng, X. Xiao, C. Huang, and C. Li, "Enhancing transient voltage quality in a distribution power system with SMES-Based DVR and SFCL," *IEEE Transactions on Applied Superconductivity*, vol. 29, no. 2, pp. 1–5, 2019.
[12] F. A. L. Jowder, "Design and analysis of dynamic voltage restorer for deep voltage sag and harmonic compensation," *IET Generation, Transmission & Distribution*, vol. 3, no. 6, pp. 547–560, 2009.
[13] A. K. Jindal, A. Ghosh, and A. Joshi, "Critical load bus voltage control using DVR under system frequency variation," *Electric Power Systems Research*, vol. 78, no. 2, pp. 255–263, 2008.
[14] N. J. Woodley, L. Morgan, and A. Sundaram, "Experience with an inverter-based dynamic voltage restorer," *IEEE Power Engineering Review*, vol. 17, no. 9, p. 43, 1997.
[15] R. Gupta and S. Gupta, "State of the art: dynamic voltage restorer for power quality improvement," *Electrical & Computer Engineering: International Journal*, vol. 4, no. 2, pp. 79–98, 2015.
[16] A. V. Borakhade and S. A. Borakhade, "Compensation of voltage sags and swells by using Dynamic Voltage Restorer (DVR)," in *Proceedings of the 2016 International Conference on Electrical, Electronics, and Optimization Techniques (ICEEOT)*, no. 2, pp. 1515–1519, Chennai, India, 2016.
[17] H. Chaudhary, "Analysis, modeling and simulation of dynamic voltage restorer (DVR) for compensation of voltage for sag-swell disturbances," *IOSR Journal of Electrical and Electronics Engineering*, vol. 9, no. 3, pp. 36–41, 2014.
[18] M. M. Mahmoud, M. K. Ratib, I. J. I, J. Swaminathan, M. M. Aly, and A. M. M. Abdel-Rahim, "Application of grey wolf optimization for PMSG-based WECS under different operating conditions: performance assessment," in *Proceedings of the 2021 Innovations in Power and Advanced Computing Technologies (i-PACT)*, Kuala Lumpur, Malaysia, November 2021.
[19] R. Mali, N. Adam, A. Satpaise, and A. P. Vaidya, "Performance comparison of two level inverter with classical multilevel inverter topologies," in *Proceedings of the 2019 IEEE International Conference on Electrical, Computer and*

Communication Technologies (ICECCT), pp. 1–7, Erode, India, September 2019.
[20] A. Bughneda, M. Salem, A. Richelli, D. Ishak, and S. Alatai, "Review of multilevel inverters for PV energy system applications," *Energies*, vol. 14, no. 6, pp. 1585–1607, 2021.
[21] J. Buczek and V. Ivankevych: Practical utility PV multilevel inverter solutions, 2021, https://arxiv.org/abs/2101.11524.
[22] A. Hassan, X. Yang, W. Chen, and M. A. Houran, "A state of the art of the multilevel inverters with reduced count components," *Electronics*, vol. 9, no. 11, pp. 1924–1927, 2020.
[23] A. S. Yusuf and I. Yusuf, "Performance analysis of photovoltaic systems using (RAMD) analysis," *Journal of the Nigerian Society of Physical Sciences*, vol. 3, no. 3, pp. 172–180, 2021.
[24] S. Seme, K. Sredenšek, B. Štumberger, and M. Hadžiselimović, "Analysis of the performance of photovoltaic systems in Slovenia," *Solar Energy*, vol. 180, pp. 550–558, 2019.
[25] R. K. Navdeep Kaur Brar, "Power quality improvement by using various voltage sag and swell controller," *International Journal of Advanced Research in Electrical, Electronics and Instrumentation Engineering*, vol. 4, no. 8, pp. 6970–6980, 2015.
[26] R. E. Nambiar, M. M, B. B, P. K. Aj, and V. Priyadarshini, "Comparative study between different controllers of DVR for power quality improvement," in *Proceedings of the 2021 International Conference on Design Innovations for 3Cs Compute Communicate Control (ICDI3C)*, pp. 84–87, Bangalore, India, 2021.
[27] E. Ancillotti, R. Bruno, and M. Conti, "The role of communication systems in smart grids: architectures, technical solutions and research challenges," *Computer Communications*, vol. 36, no. 17-18, pp. 1665–1697, 2013.
[28] R. El-Azab, "Smart homes: potentials and challenges," *Clean Energy*, vol. 5, no. 2, pp. 302–315, 2021.
[29] D. Marikyan, S. Papagiannidis, and E. Alamanos, "A systematic review of the smart home literature: a user perspective," *Technological Forecasting and Social Change*, vol. 138, pp. 139–154, 2019.
[30] S. Sun, Z. Cao, H. Zhu, and J. Zhao, "A survey of optimization methods from a machine learning perspective," *IEEE Transactions on Cybernetics*, vol. 50, no. 8, pp. 3668–3681, 2020.
[31] M. M. Mahmoud, M. M. Aly, H. S. Salama, and A.-M. M. Abdel-Rahim, "Dynamic evaluation of optimization techniques–based proportional–integral controller for wind-driven permanent magnet synchronous generator," *SAGE Journal*, vol. 45, no. 3, 2020.
[32] M. M. Mahmoud, M. K. Ratib, M. M. Aly, and A. M. M. Abdel–Rahim, "Application of whale optimization technique for evaluating the performance of wind-driven PMSG under harsh operating events," *Process Integration and Optimization for Sustainability*, vol. 6, no. 2, pp. 447–470, 2022.
[33] Z. Wu, S. Pan, F. Chen, G. Long, C. Zhang, and P. S. Yu, "A comprehensive survey on graph neural networks," *IEEE Transactions on Neural Networks and Learning Systems*, vol. 32, no. 1, pp. 4–24, 2021.
[34] H. B. Patel and S. N. Chaphekar, "Developments in PID controllers: literature survey," *International Journal of Engineering Innovation and Research*, vol. 1, no. 5, pp. 425–430, 2012.
[35] A. Padmanaban and S. Padmanaban, "Dynamic voltage restorer (DVR): a comprehensive review of topologies, power converters, control methods, and modified configurations," *Energies*, vol. 13, no. 16, Article ID 4152, 2020.
[36] E. M. Kuo and C. C. Kuo, "Voltage sag enhancement of grid connected hybrid PV-wind power system using battery and SMES based dynamic voltage restorer," *IEEE Access*, vol. 8, pp. 130003–130013, 2020.
[37] C. Tu, Q. Guo, F. Jiang, H. Wang, and Z. Shuai, "A comprehensive study to mitigate voltage sags and phase jumps using a dynamic voltage restorer," *IEEE Journal of Emerging and Selected Topics in Power Electronics*, vol. 8, no. 2, pp. 1490–1502, 2020.
[38] S. C. Yáñez-Campos, G. Cerda-Villafaña, and J. M. Lozano-García, "A two-grid interline dynamic voltage restorer based on two three-phase input matrix converters," *Applied Sciences*, vol. 11, no. 2, pp. 561–585, 2021.
[39] C. Tu and J. GuoJiangChenLiXiaoGao, "Dynamic voltage restorer with an improved strategy to voltage sag compensation and energy self-recovery," *CPSS Transactions on Power Electronics and Applications*, vol. 4, no. 3, pp. 219–229, 2019.
[40] F. Jiang, C. Tu, Q. Guo, Z. Shuai, X. He, and J. He, "Dual-functional dynamic voltage restorer to limit fault current," *IEEE Transactions on Industrial Electronics*, vol. 66, no. 7, pp. 5300–5309, 2019.
[41] F. B. Moreno, J. E. Palacios, J. Posada, and J. A. Lopez, "Implementation and evaluation of a new DVR topology with AC link for series compensation," *Electric Power Systems Research*, vol. 181, Article ID 106184, 2020.
[42] M. I. Mosaad, M. O. Abed El-Raouf, M. A. Al-Ahmar, and F. M. Bendary, "Optimal PI controller of DVR to enhance the performance of hybrid power system feeding a remote area in Egypt," *Sustainable Cities and Society*, vol. 47, Article ID 101469, 2019.
[43] D. V. Tien, R. Gono, and Z. Leonowicz, "A multifunctional dynamic voltage restorer for power quality improvement," *Energies*, vol. 11, no. 6, pp. 1351–1367, 2018.
[44] A. Benali, M. Khiat, T. Allaoui, and M. Denai, "Power quality improvement and low voltage ride through capability in hybrid wind-PV farms grid-connected using dynamic voltage restorer," *IEEE Access*, vol. 6, pp. 68634–68648, 2018.
[45] E. Farhadi Kangarlu and M. Farhadi Kangarlu, "Voltage quality improvement by a dynamic voltage restorer based on a direct three-phase converter with fictitious DC link," *IET Generation, Transmission & Distribution*, vol. 5, no. 8, pp. 814–823, 2011.
[46] H. C. Sanjay and G. Gaurav, "Mitigation of voltage sag/swell using dynamic voltage restorer (DVR)," *IOSR Journal of Electrical and Electronics Engineering*, vol. 8, no. 4, pp. 21–38, 2013.
[47] D. Datta, S. R. Fahim, S. K. Sarker, S. M. Muyeen, M. R. Islam Sheikh, and S. K. Das, "A robust control method for damping and tracking of secondary network voltage of a PV based hybrid AC/DC microgrid," *Frontiers in Energy Research*, vol. 7, 2020.
[48] A. Chouder, S. Silvestre, B. Taghezouit, and E. Karatepe, "Monitoring, modelling and simulation of PV systems using LabVIEW," *Solar Energy*, vol. 91, pp. 337–349, 2013.
[49] S. K. Biswas and S. Biswas, "Fuzzy logic and PI controller implementation on dynamic voltage restorer," in *Proceedings of the 2021 2nd Global Conference for Advancement in Technology (GCAT)*, Bangaluru, India, 2021.
[50] B. Jaganathan, R. Sharanya, S. K. Devi, and S. K. Sah, "Ziegler-Nichol's method of online tuning of PMSM for improved transient response," in *Proceedings of the 2010 International*

Conference on Power, Control and Embedded Systems, Allahabad, India, 2010.

[51] L. Rout and U. K. Rout, "Optimal control of a high gain DC-DC converter," *International Journal of Power Electronics and Drive Systems*, vol. 13, no. 1, pp. 256–266, 2022.

[52] Z. Yu, X. Shi, J. Zhou, X. Chen, and X. Qiu, "Effective assessment of blast-induced ground vibration using an optimized random forest model based on a Harris hawks optimization algorithm," *Applied Sciences*, vol. 10, no. 4, Article ID 1403, 2020.

[53] P. Kumar, S. N. Singh, and S. Dawra, "Software component reusability prediction using extra tree classifier and enhanced Harris hawks optimization algorithm," *International Journal of System Assurance Engineering and Management*, vol. 13, no. 2, pp. 892–903, 2022.

[54] A. A. Heidari, S. Mirjalili, H. Faris, I. Aljarah, M. Mafarja, and H. Chen, "Harris hawks optimization: algorithm and applications," *Future Generation Computer Systems*, vol. 97, pp. 849–872, 2019.

[55] V. Blažek, M. Petružela, T. Vantuch, S. Mišák, Z. Slanina, and W. Walendziuk, "An appliance impact estimation on power quality parameters in microgrid environment," in *Proceedings of the 9th Innovations-Sustainability-Modernity-Openness Conference (ISMO'20)*, August 2020.

[56] A. Soukkou, M. C. Belhour, and S. Belhour, "Review, Design, optimization and stability analysis of fractional-order PID controller," *International Journal of Intelligent Systems and Applications*, vol. 8, no. 7, pp. 73–96, 2016.

[57] P. Zhou, X. Hu, Z. Zhu, and J. Ma, "What is the most suitable Lyapunov function?" *Chaos, Solitons & Fractals*, vol. 150, Article ID 111154, 2021.

[58] P. Fernandez-Comesana, F. D. Freijedo, J. Doval-Gandoy, O. Lopez, A. G. Yepes, and J. Malvar, "Mitigation of voltage sags, imbalances and harmonics in sensitive industrial loads by means of a series power line conditioner," *Electric Power Systems Research*, vol. 84, no. 1, pp. 20–30, 2012.

[59] V. S. Phadke and S. B. Phadke, "Control of uncertain nonlinear systems using an uncertainty and disturbance estimator," *Journal of Dynamic Systems, Measurement, and Control*, vol. 134, no. 2, 2 pages, 2012.

[60] Y. Wang, B. Ren, and Q. C. Zhong, "Robust power flow control of grid-connected inverters," *IEEE Transactions on Industrial Electronics*, vol. 63, no. 11, pp. 6887–6897, 2016.

[61] E. F. de Oliveira, M. E. de Lima Tostes, C. A. O. de Freitas, and J. C. Leite, "Voltage THD analysis using knowledge discovery in databases with a decision tree classifier," *IEEE Access*, vol. 6, pp. 1177–1188, 2018.